Dynamic permeability due to physical coupling of reactive CO_2-flow and deformation

Nina Simon[1,2]

Yuri Y. Podladchikov[3] and Harald Johansen[1]

[1]Miljøteknologi, Institutt for Energiteknikk, Kjeller, Norway
[2]Institutt for geovitenskap, Universitetet i Bergen, Norway
[3]Faculté des géosciences et de l'environnement, Université de Lausanne, Switzerland

Outline

1) Evidence for dynamic permeability from data
2) What causes dynamic permeability?
    1) Permeability variations in space: pre-existing heterogeneity
    2) Permeability changes in time (and space):
        1) Fracturing/rock failure
        2) Dissolution
        3) Elastic response to stress changes
        4) Compaction: elastic, plastic, viscous
        5) Precipitation
3) How to model dynamic permeability during flow in a reservoir?
4) The porosity wave model: captures opening and closing of porosity as a response to variations in effective pressure (and reactions).
5) At which parameters do we expect porosity waves to occur in CO_2 storage operations?

Dynamic permeability: evidence from data

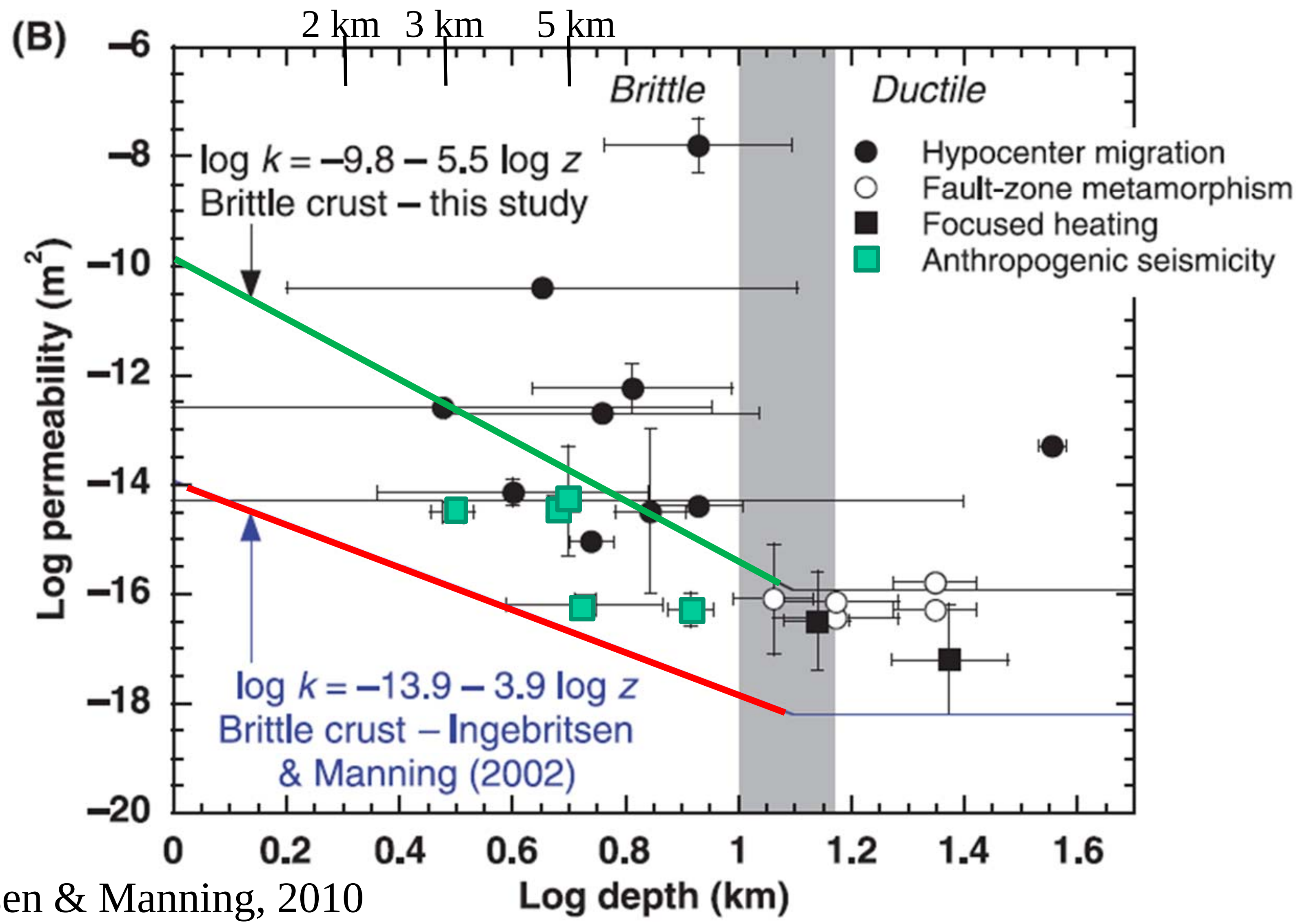

Ingebritsen & Manning, 2010

Dynamic permeability: evidence from data

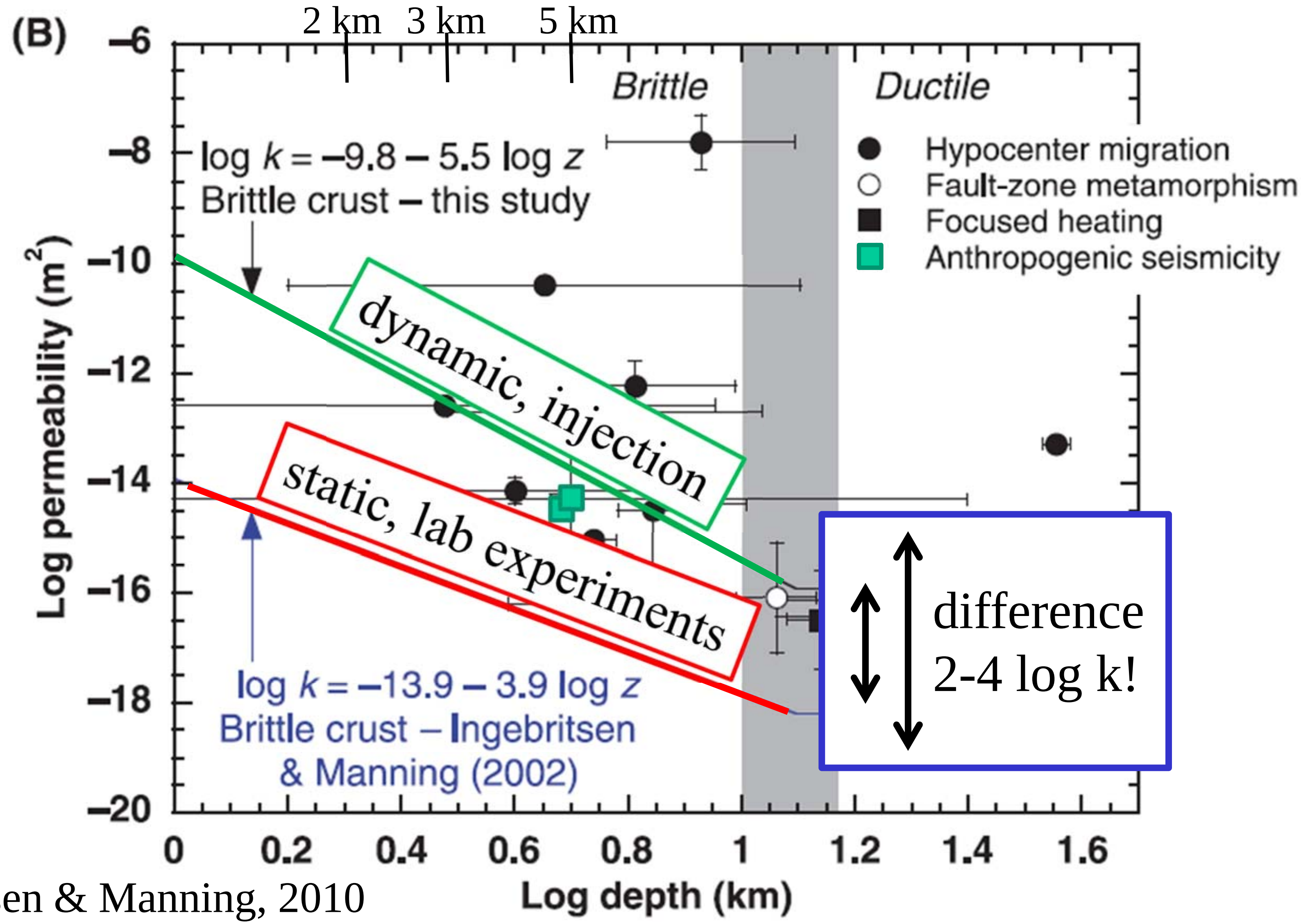

Ingebritsen & Manning, 2010

Opening of pore space: permeability increase

(Micro)fracturing

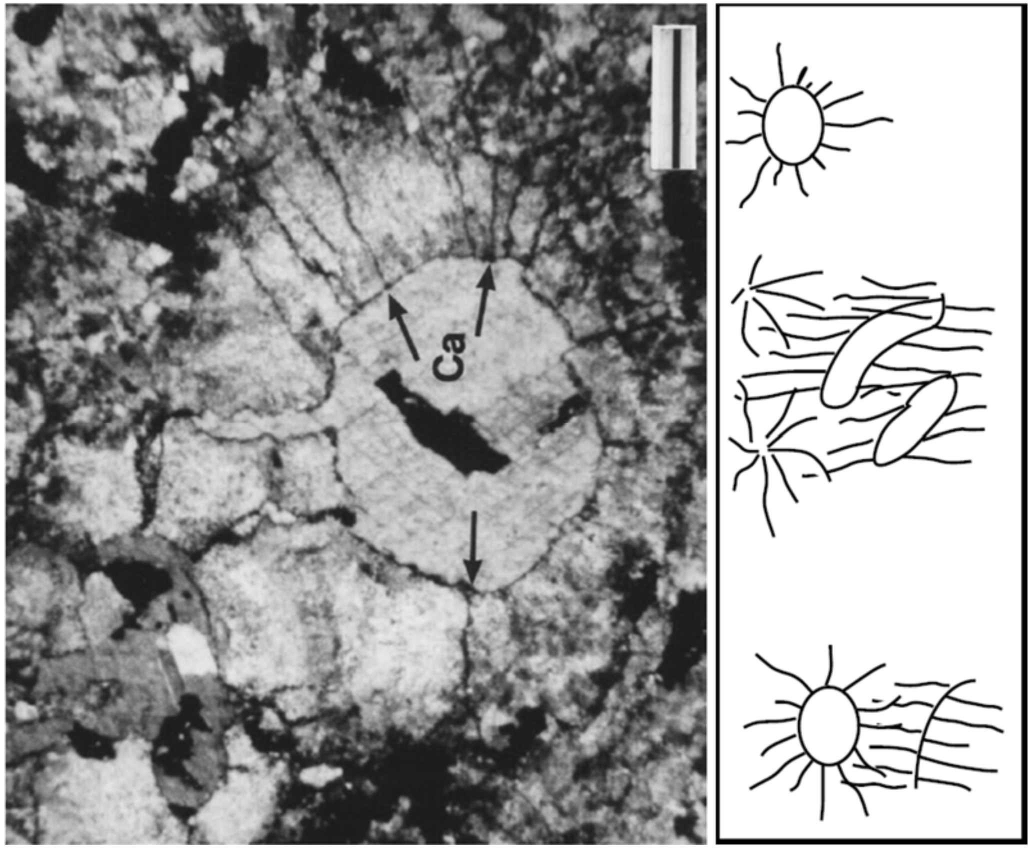

Radial microfractures Upper Devonian reservoirs, deep Alberta basin (Márquez and Mountjoy, 1996).

Dissolution

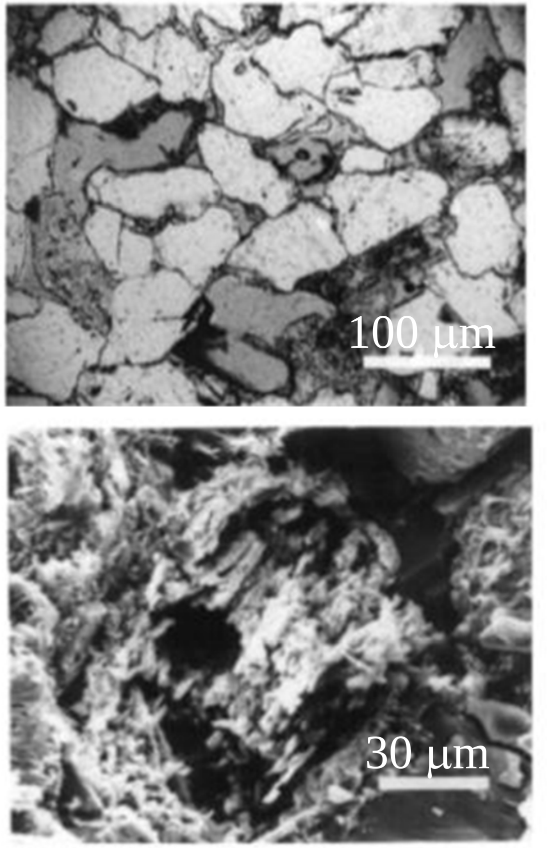

Figure 3—Scanning electron microscopy (SEM) and thin-section photomicrographs from well 22/30a-1 showing extensive secondary porosity. (a) Thin-section photomicrograph (plane-polarized light) showing several secondary pores after feldspar; scale bar = 100 µm, depth 4665.8 m. (b) SEM photomicrograph showing a highly corroded alkali feldspar; scale bar = 30 µm, depth 4657.2 m.

Wilkinson et al., 1997

Closure of pore space: permeability decrease

Flow-reaction-deformation experiments show closure of pores/fractures by pressure solution creep and compaction

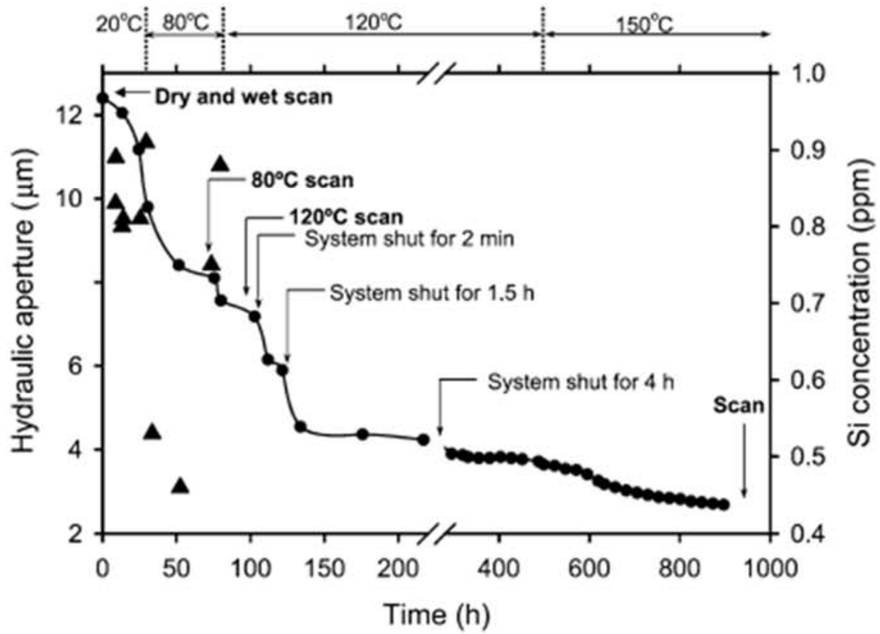

Figure 4
Change in hydraulic aperture with time for a circulation test on a fracture in novaculite. Test is conducted at incremented temperatures but constant stress (Polak *et al.*, 2003).

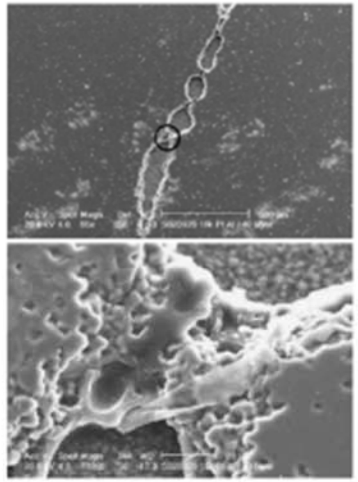

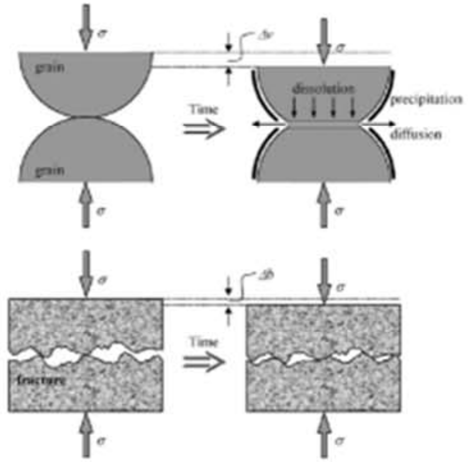

Polak et al., 2003; Yasuhara et al., 2004; Elsworth and Yasuhara, 2006

What is the effect of coupled fluid flow, deformation (elastic and microfracturing) and reactions (chemical compaction)?

➔ dynamic opening and closure of pores and therefore permeability changes

➔ dynamic reorganization of flow

How can we model all this in ONE continuum model?

Porosity waves: fluid flow in a deformable medium

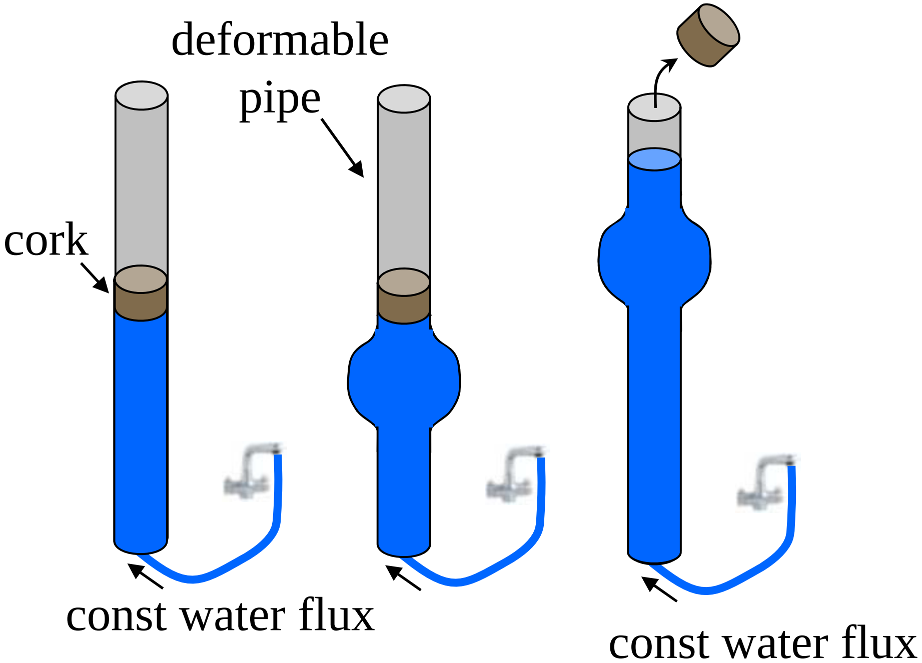

Flow is driven by a pressure difference (in the simplest case buoyancy) and by compaction of the pores. Non-linear coupling between porosity and permeabilty and permeability and pressure leads to instabilities and focusing of flow.

Equations (and assumptions)

Mass balance

$$\frac{\partial(1-\varphi)}{\partial t}+\nabla((1-\varphi)v_s)=0 \qquad \frac{\partial\varphi}{\partial t}+\nabla(\varphi v_f)=0 \qquad \frac{d\rho_s}{dt}=\frac{d\rho_f}{dt}=0$$

solid   fluid

Force balance

$$\frac{\partial\bar{\sigma}_{ij}}{\partial x_j}=\frac{\partial\sigma_{ij}^{eff}}{\partial x_j}-\frac{\partial p_f}{\partial x_i}=g\left[(1-\varphi)\rho_s+\varphi\rho_f\right]\hat{z} \qquad P_{eff}=P_f-\overline{P}$$

Darcy's law

$$\varphi(v_f-v_s)=-\frac{k(\varphi)}{\mu_f}\nabla\left(p_f+\rho_f gz\right)$$

Rheology

$$\frac{1}{\varphi(1-\varphi)}\frac{d\varphi}{dt}=\underbrace{\frac{P_{eff}}{\eta(\varphi,P_{eff})}}_{\text{visco-plastic}}+\underbrace{\frac{1}{\beta(\varphi)}\frac{dP_{eff}}{dt}}_{\text{elastic}}$$

Yarushina, 2010

Simplified and in 1D: 2 equations, 2 unknowns

$$\text{I} \quad \frac{\partial\varphi}{\partial t}=-\frac{\partial}{\partial z}\left(\frac{k(\varphi)}{\mu_f}\cdot\left(\frac{\partial P_e}{\partial z}+\Delta\rho g\right)\right) \qquad \text{II} \quad \frac{\partial P_e}{\partial t}=\frac{1}{\beta(\varphi)}\left(\frac{\partial\varphi}{\partial t}-\frac{P_e}{\eta(\varphi)}\right)$$

$$k(\varphi)=k_0\cdot\left(\frac{\varphi}{\varphi_0}\right)^n,\ n=3;\ \beta(\varphi)=\varphi^b\cdot\beta_0,\ b=1/2 \text{ and } \eta(\varphi)=\eta_s/\varphi^m,\ m=1.$$

Modeling deformation and fluid flow

visco-elastic porosity waves, 2D

initial condition

effective pressure | porosity | effective pressure | porosity

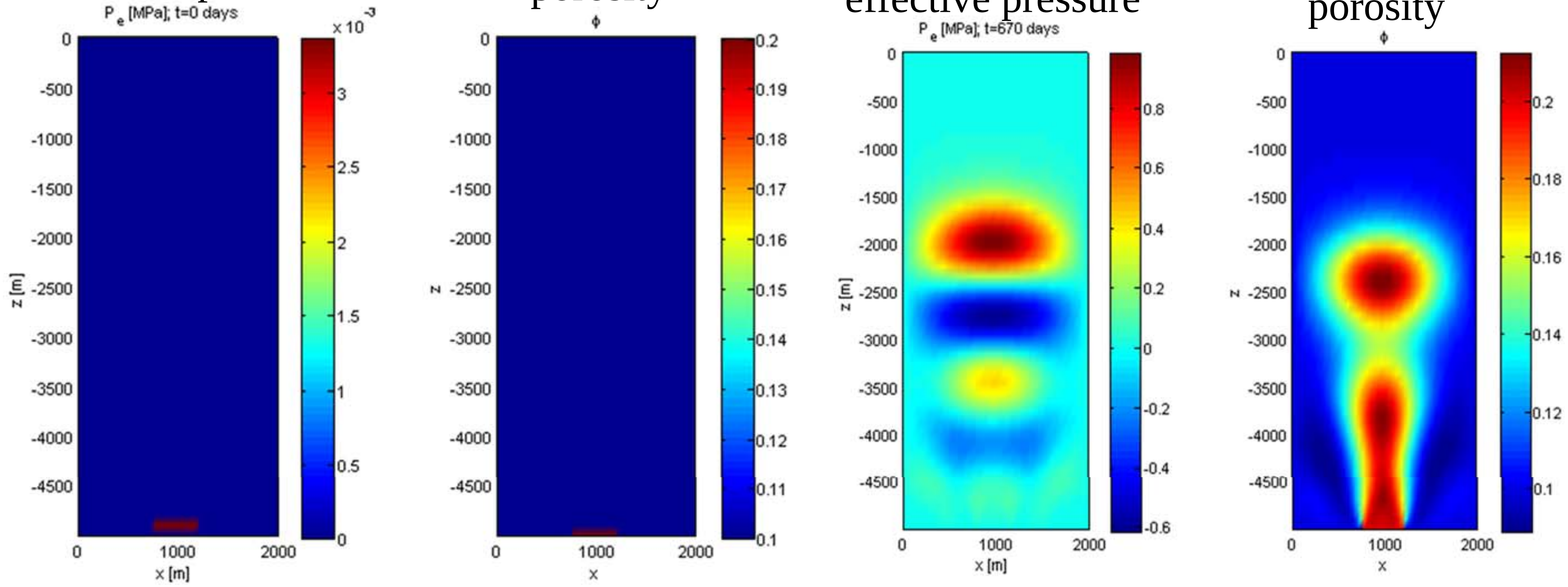

Rheology: opening of pores much easier than closure

Viscous linear

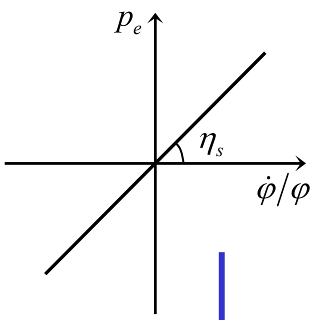

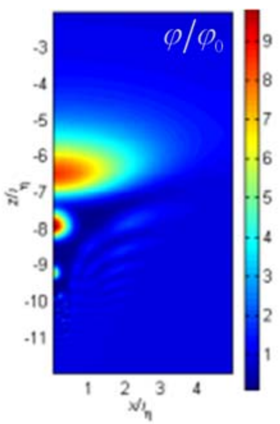

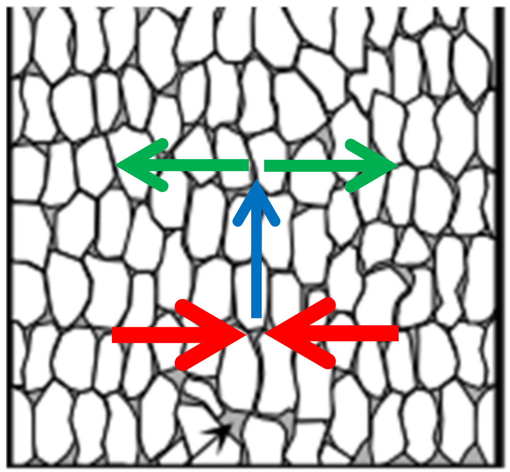

from 'blob'
to 'jet'
(or channel)

Connolly & Podladchikov, 1998

Viscous bilinear

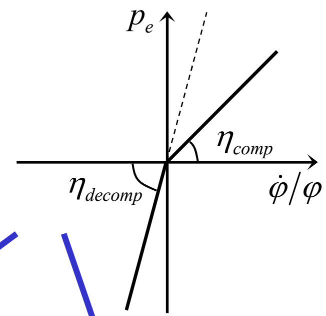

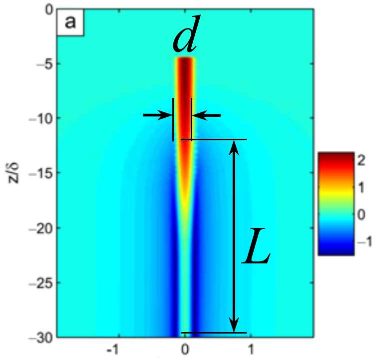

$L/d = \delta$

$\delta = f\left(\eta_{comp}/\eta_{decomp}\right)$

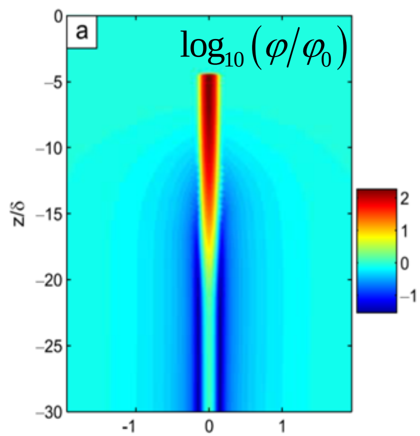

Connolly & Podladchikov, 2007

Modeling deformation and fluid flow

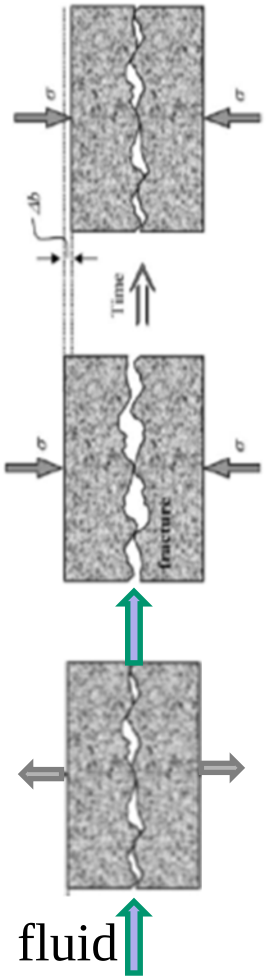

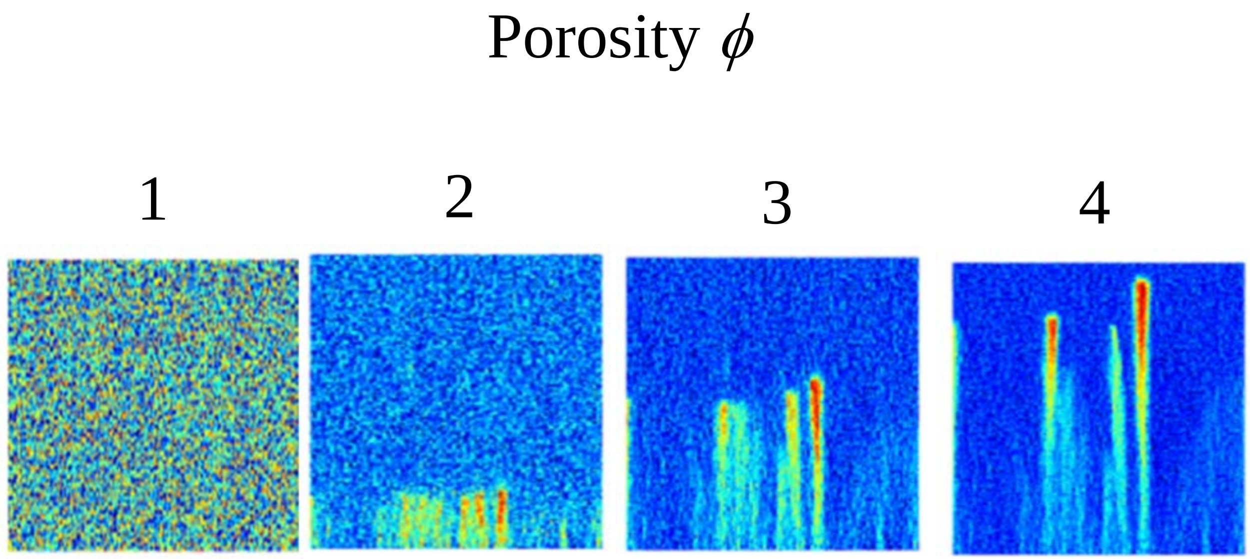

Modeling deformation and fluid flow

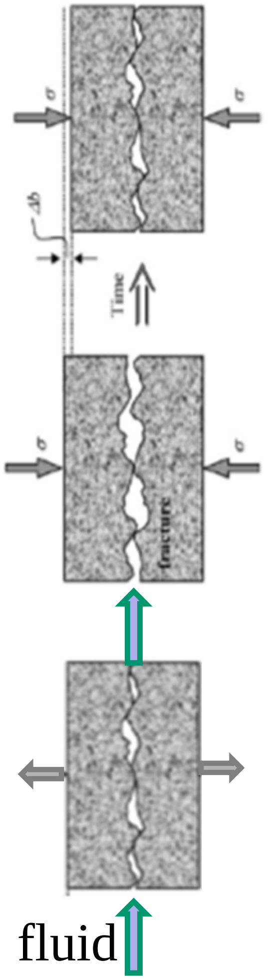

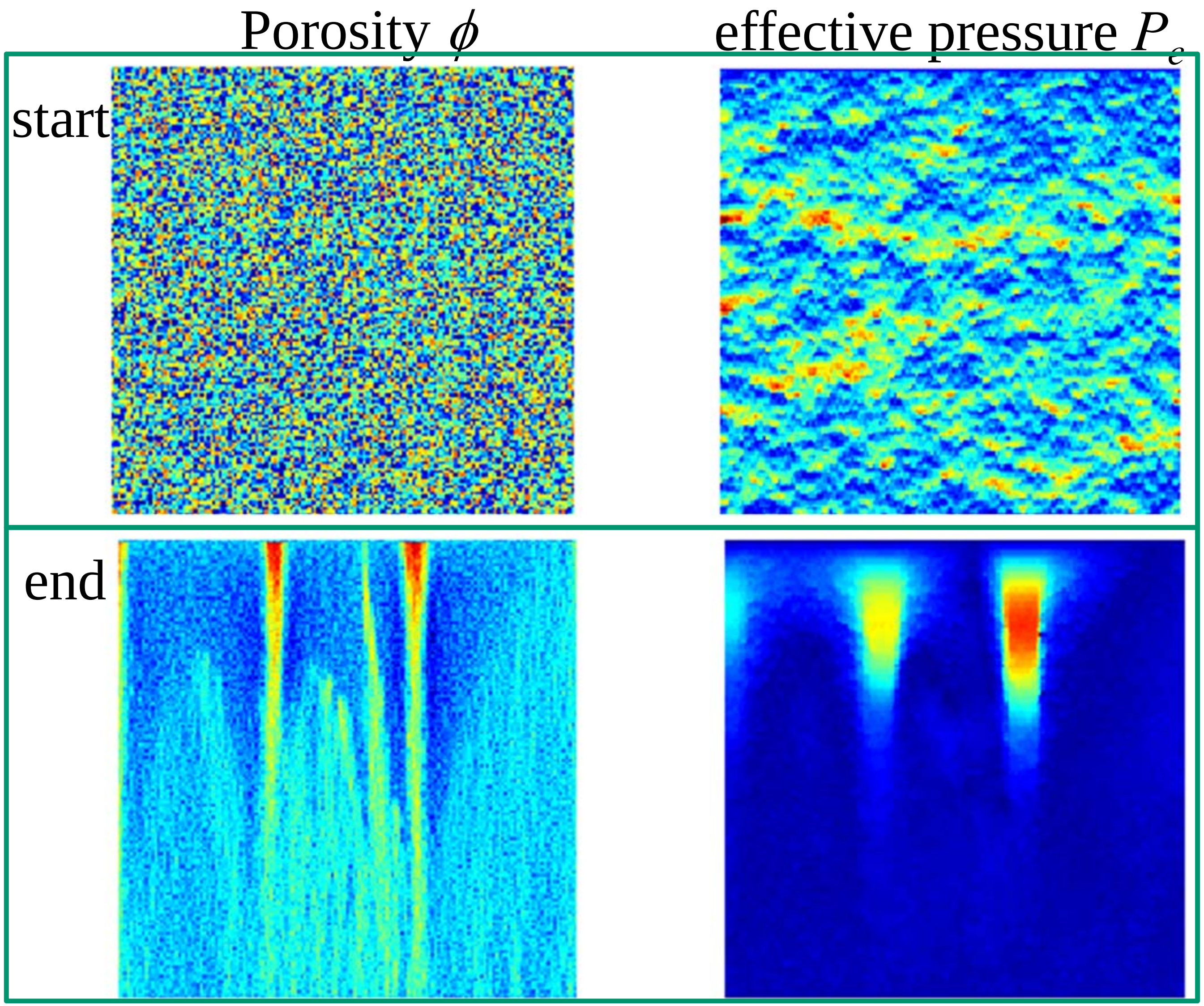

Porosity waves: relevant for CO_2 storage?

Dimensional analysis and parameter-check

Characteristic length-scale: compaction length $L^* = \sqrt{\frac{k_0 \eta_s}{\varphi_0 \mu_f}}$

Characteristic pressure $p^* = \Delta \rho g^* L^*$

Characteristic time $t^* = \eta_s / p^*$

with $k_0 \approx 10^{-15} m^2$, $\varphi_0 \approx 0.1$, $\mu_f \approx 10^{-4} Pa \cdot s$ we need

$\eta_s \approx 10^{15} Pa \cdot s$

to get $L^* = 100 m$ and $t^* = 21 years$

If η_{decomp}=0.1-0.0001 η_{comp}, and/or p^* is higher than buoyancy pressure, timescales will reduce significantly.

Reaction-induced viscosity from experiments

Le Guen et al., 2007

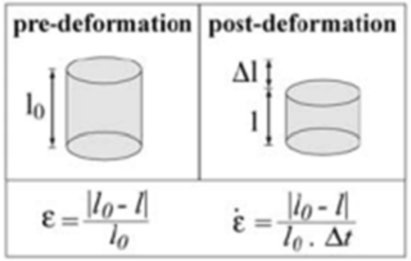

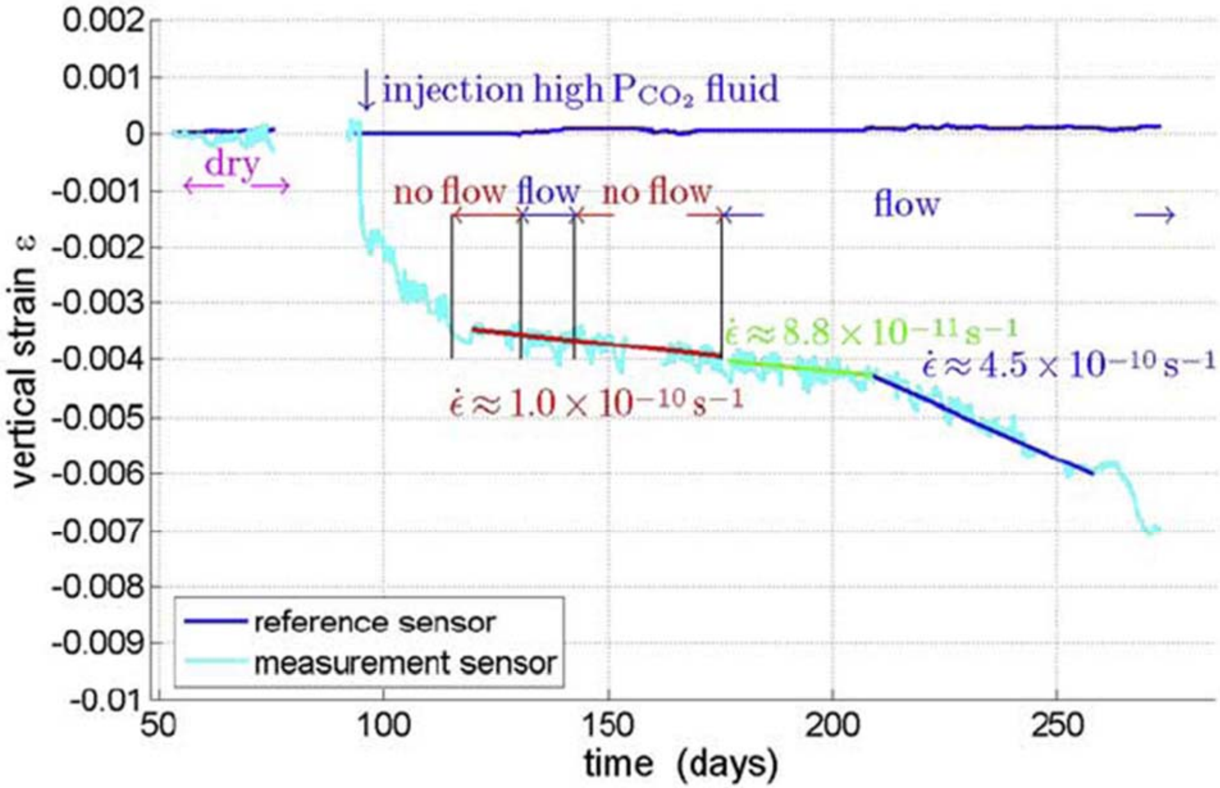

Figure 5. Vertical axial strain deformation measured for Lavoux W526 sample in the absence of fluid and during injection of high P_{co_2} saline fluid (cyan curve). Time periods with no data represent non-stable conditions associated with parameter changes. The red time period $\dot{\epsilon}$ includes a short flow period. Note that the renewed injection of high P_{co_2} saline solution caused a large increase in $\dot{\epsilon}$, but after time lag of ≈40 days. The end of the experiment was marked by a sudden, rapid increase in strain and strain rate.

Reaction-induced viscosity from experiments

Le Guen et al., 2007

Table 2. Experimental Parameters During Compaction

Rock sample	Estaillades		Lavoux W526	Lavoux W520	Sandstone
Fluid P_{CO_2}	low P_{CO_2}	high P_{CO_2}	high P_{CO_2}	low P_{CO_2}	high P_{CO_2}
σ_1 (MPa)	8.9	10.0	16.3	16.3	16.0
σ_3 (MPa)	7.3	8.5	12.0	11.6	10.2
p_f (MPa)	5.9	7.8	7.9	7.9	8.3
σ_e (MPa)	3.0	2.2	8.4	8.4	7.7
P_{CO_2} (MPa)	$10^{-4.5}$	7.8	7.9	$10^{-4.5}$	8.3
T (°C)	25	80	40	40	40
[NaCl] (mol l^{-1})	0	0	10^{-2}	10^{-2}	10^{-2}
Fluid flow (m^3 s^{-1})	8.33×10^{-11}	8.33×10^{-11}	8.33×10^{-11}	8.33×10^{-11}	8.33×10^{-11}
Residence time (h)	20.5	20.5	12.8	14.0	10.0
Fluid velocity (m s^{-1})	6×10^{-7}	6×10^{-7}	1×10^{-6}	9×10^{-7}	1.4×10^{-6}

Table 3. Average Strain Rates With Indicated Time Ranges

	Dry (s^{-1})	Low P_{CO_2} fluid flow (s^{-1})	Low P_{CO_2} no flow (s^{-1})	High P_{CO_2} fluid flow (s^{-1})	High P_{CO_2} no flow (s^{-1})
Estaillades	1.0×10^{-12}	1.9×10^{-11}	–	1.0×10^{-10}	3.0×10^{-11}
	days 35–58	days 198–221	–	days 366–370	days 475–495
Lavoux-W526	≈0	–	–	4.5×10^{-10}	1.0×10^{-10}
	day 53–74			day 209–258	day 120–175
Lavoux-W520	1.1×10^{-11}	2.6×10^{-10}	8.1×10^{-11}	–	–
	day 26–41	day 231–282	day 200–230		
Sandstone	–	–	–	2.3×10^{-11}	4.6×10^{-12}
				day 59–134	day 153–161

Reaction-induced viscosity from experiments

Le Guen et al., 2007

Table 2. Experimental Parameters During Compaction

Rock sample	Estaillades		Lavoux W526	Lavoux W520	Sandstone
Fluid P_{CO_2}	low P_{CO_2}	high P_{CO_2}	high P_{CO_2}	low P_{CO_2}	high P_{CO_2}
σ_1 (MPa)	8.9	[illegible]	[illegible]	16.3	16.0
σ_3 (MPa)	7.3	[illegible]	[illegible]	11.6	10.2
p_f (MPa)	5.9	[illegible]	[illegible]	7.9	8.3
σ_e (MPa)	3.0	[illegible]	[illegible]	8.4	7.7
P_{CO_2} (MPa)	10^{-4}	[illegible]	[illegible]	$10^{-4.5}$	8.3
T (°C)	25	[illegible]	[illegible]	40	40
[NaCl] (mol l^{-1})	0	[illegible]	[illegible]	10^{-2}	10^{-2}
Fluid flow ($m^3\ s^{-1}$)	8.33 × 1	[illegible]	[illegible]	8.33×10^{-11}	8.33×10^{-11}
Residence time (h)	20.5	[illegible]	[illegible]	14.0	10.0
Fluid velocity ($m\ s^{-1}$)	6 × 10	[illegible]	[illegible]	9×10^{-7}	1.4×10^{-6}

Table 3. Average Strain Rates With I

	Dry (s^{-1})	Low	[illegible]	fluid flow (s^{-1})	High P_{CO_2} no flow (s^{-1})
Estaillades	1.0×10^{-12} days 35–58	[illegible]	[illegible]	$\times 10^{-10}$ 366–370	3.0×10^{-11} days 475–495
Lavoux-W526	≈0 day 53–74	[illegible]	[illegible]	$\times 10^{-10}$ 209–258	1.0×10^{-10} day 120–175
Lavoux-W520	1.1×10^{-11} day 26–41	2.6 × 10 day 231–282	8.1 × 10 day 200–230	–	–
Sandstone	–	–	–	2.3×10^{-11} day 59–134	4.6×10^{-12} day 153–161

Linear viscosity:

$$\sigma = \mu \cdot \dot{\varepsilon}$$

$$\mu = \sigma / \dot{\varepsilon}$$

$$\mu = 16 \cdot 10^{6}\,Pa / 2.3 \cdot 10^{-11}\,s^{-1}$$

$$\underline{\mu \approx 10^{17}\,Pa \cdot s}$$

at 40˚C for sandstone

Summary

- Permeability is expected to change dynamically in a reservoir during flow, in particular if reactive CO_2-rich fluids are involved.
- Coupling between flow, reactions and deformation leads to effectively visco-elasto-plastic rheology.
- Fluid focusing due to non-linear coupling leading to instabilities can be modeled as porosity waves.
- Preliminary results indicate that porosity waves/ fluid focusing and enhanced tranport may occur in reservoir operations, in particular in low-permeability rocks.

➔ This may enhance injectivity, but also increase the risk for leakage.

➔ We need more theoretical and experimental investigations of coupled fluid flow, reactions and deformation, and comparison to reservoir data.